From grains to planetesimals : the microphysics of dust coagulation

Krijt, S.

Author: Krijt, Sebastiaan
Title: From grains to planetesimals: the microphysics of dust coagulation
Issue Date: 2015-04-29

1

Introduction

We live in an exciting time. The discovery of an enormous number of exoplanets (planets that revolve around stars other than the Sun) marks one of the most important scientific findings of this age. Since the detection of the first exoplanet around a main-sequence star approximately 20 years ago (Mayor & Queloz 1995), over 1800 have now been detected, and it is becoming clear that the universe is teeming with planets. On average, every star has a planetary system, and every 5th Sun-like star is orbited by an Earth-like planet.

Already in 1695, Dutch astronomer Christiaan Huygens reached a similar conclusion, though not supported by observations. In his *Cosmotheoros*, he wrote:

> "What a wonderful and amazing Scheme have we here of the magnificent Vastness of the Universe! So many Suns, so many Earths, and every one of them stock'd with so many Herbs, Trees and Animals, and adorn'd with so many Seas and Mountains! And how must our wonder and admiration be encreased when we consider the prodigious distance and multitude of the Stars?"

Huygens' vision was spot on. Little over three centuries later, we have indeed discovered many Suns and many Earths. On planets we could study up close, we have discovered Seas (though none of them made of liquid water) and Mountains.

But we have discovered more than just Earths; we have discovered a very diverse population of exoplanets. Fig. 1.1 shows the masses and semi-major axes of all known exoplanets as of January 13, 2015. The Earth ($\oplus$) and the Jovian planets (Jupiter, Saturn, Uranus, and Neptune) are shown for comparison. Planets appear to come in a lot of varieties; some very massive and on very wide orbits, others much smaller and on orbits with periods of only several days. Of particular interest are planets that are located in the *habitable zone*, i.e., at a distance from their star where the temperature is such that

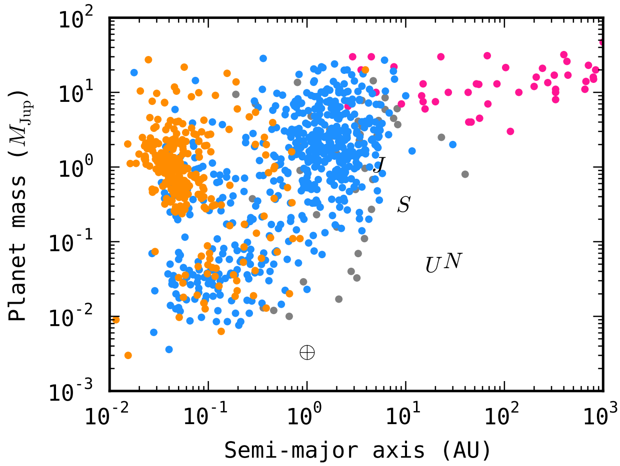

Figure 1.1: Mass and separation of all 1876 exoplanets known as of January 13, 2015. Color-coding indicates detection method: transit (•); radial velocity (•); direct imaging (•); and other methods (•). The Earth and Jovian planets are indicated as well. Data from `http://exoplanet.eu/`.

it allows the presence of liquid water. As of January 2015, 8 small rocky exoplanets have been discovered that lie in the habitable zone of their parent star, and it is estimated that 22% of Sun-like stars have a Earth-sized planet orbiting within their habitable zone (Petigura et al. 2013). If life elsewhere resembles life as we know it, these worlds should be good places to look for Huygens' Herbs, Trees, and Animals.

With the realization that planetary systems are common and planets in the habitable zone are widespread, come questions about their formation. How are planets made? What determines their characteristics? Today, astronomers have a coarse picture of how planets are created, though many details prove elusive. The general paradigm dictates that planet formation takes place inside protoplanetary disks, the left-overs of the star formation process. These disks, with sizes up to several 100 AU, consist of mostly hydrogen gas, and live for several million years. In the disk, the wide variety of gas densities, temperatures, and intensities of stellar radiation, give rise to complex chemistry, and the presence of many different molecules, including water, has been confirmed observationally in disks around young stars. A small fraction of the disk's mass (~1%) is accounted for by microscopic dust particles. Suspended in the gaseous nebula, these dust particles collide and coalesce, growing into aggregates, then boulders, planetesimals, and eventually planetary embryos. The embryos have sufficient gravity to capture gas from the nebula, and start to form primitive atmospheres. Eventually, the embryos merge to form fully-grown planets. The full journey from dust grain to planet constitutes an increase in mass of over 36 orders of magnitude, and takes place over millions of years.

The key unanswered questions in planet formation are then: what are the key processes that make this growth possible, and how do they depend on environment? What is the inventory of planets, and in particular, of planets in the habitable zone? Focussing on the planet's atmosphere and potential to harbor life: what are the principle sources of organics and volatiles, and what are the processes that played a role in their delivery?

In this thesis, we focus on the first - and least understood - step in the planet-formation process: the coagulation, through successive sticking collisions, of microscopic dust particles into planetary building blocks several kilometers across (planetesimals). The structure of the protoplanetary disk, as well as the composition, size, and shape of the dust particles determine the efficiency of this growth process. In particular, the dust grain *porosity* (a measure for the internal density) plays an central role. For compact particles, current theories predict several growth barriers, making it very difficult for them to gain mass and grow larger than a meter in size. In fact, were it not for the observed ubiquity of exoplanets, one might be tempted to conclude that planetesimal formation is a hopeless endeavor. However, recent studies suggest dust grains might not be compact at all, but rather form very open, porous structures. These porous aggregates behave very differently from compact ones - both aerodynamically and mechanically. As a result, some of the growth barriers that limit the growth of compact particles might not apply to highly porous ones.

The principle objective of this thesis is to understand how the microphysics of initially tiny dust grains influence their potential to coagulate into macroscopic planetesimals. In other words, how does a grain's (collisional) history determine its porosity, and how does that porosity influence the grain's future? To answer these questions, we start at the smallest scales, and slowly work our way up. Chapters 2 and 3 deal with the adhesive contact between micrometer-size spheres, and describe the forces and energies needed to break and re-arrange single adhesive bonds. In Chapter 4, porous dust coagulation is modeled in detail in a localized part of the protoplanetary nebula. Then, in Chapter 5, we address the global dust evolution in a full protoplanetary disk, directly connecting the microphysics of the growing aggregates to the eventual formation of a population of planetesimals. Chapter 6 focusses on small dust grains in evolved debris disks: the relics of planet-forming disks.

In the remainder of the introduction, the general concepts of star- and planet formation (Sect. 1.1) and the perilous journey from dust grain to planetesimal (Sect. 1.2) are described. Dust microphysics, and its importance to the early stages of planet formation, is described in Sect. 1.3, and an outline of this thesis is presented in Sect. 1.4.

1.1 Overview of the planet formation process

The standard theory of planet formation is that planets form out of a thin disk of gas and dust that surrounds young stars (Safronov 1972; Goldreich & Ward 1973). These protoplanetary disks, or accretion disks, are the natural by-products of star formation, and their structure was first described by Shakura & Sunyaev (1973) and Lynden-Bell & Pringle (1974). The main stages of star- and planet-formation, as they are believed to occur in isolated and low-mass systems, are depicted in Fig. 1.2.

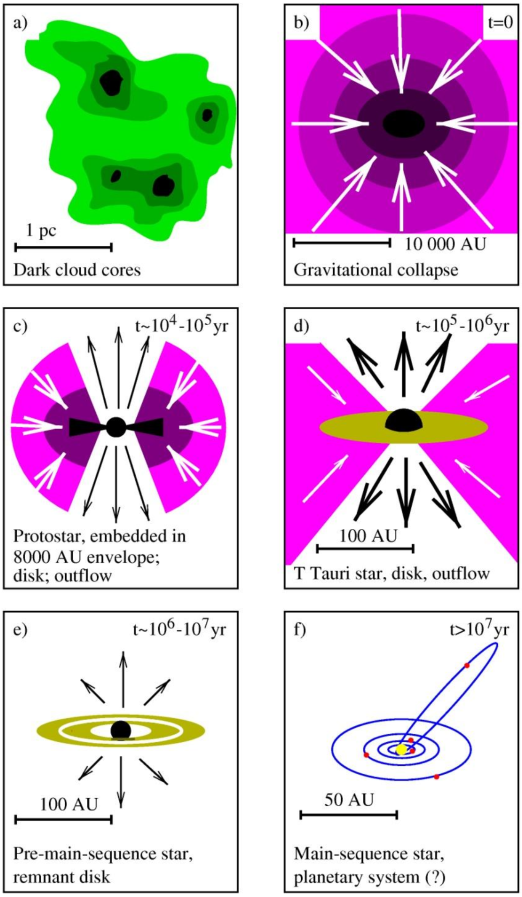

Figure 1.2: Schematic of the star- and planet formation process for low-mass stars. (a) Molecular clouds, composed of mostly hydrogen gas, form dark and cold cores. (b) When cores become massive enough, they collapse under their own gravity. (c) The cloud's non-zero angular momentum prevents the material from accreting onto the core, forming an accretion disk. The accretion rate is very high and angular momentum is removed by a (radial) outflow. (d) Accretion is slowing down, and the protoplanetary disk, with a typical size of ~100 AU is clearly visible. (e) The gas in the protoplanetary disk is slowly dissipated. At the same time, dust particles are colliding, coagulating into larger grains, and potentially forming planetary building blocks. (f) A planetary system has formed. Figure from Hogerheijde (1998), after Shu et al. (1987).

1.1.1 Protoplanetary disk formation and structure

Low-mass stars form out of the gravitational collapse of the cold, dense cores of molecular clouds (Fig. 1.2a). These cores, with sizes $\lesssim$0.1 pc, consist mainly of H_2 gas, with about 1% of their mass present in the form of dust. The temperatures are around $T \sim 10-20$ K, and gas number densities are of the order of $n \sim 10^4 - 10^5$ cm^{-3}. When such a core becomes massive enough, the gas pressure can no longer support its self-gravity, and the core will start to collapse. The critical mass above which clouds become unstable is called the Jeans mass

$$M_{\rm J} \simeq 2.9\ M_\odot \left(\frac{T}{10\ \rm K}\right)^{3/2} \left(\frac{n}{10^4\ \rm cm^{-3}}\right)^{-1/2}. \tag{1.1}$$

Thus, the typical mass of an unstable core is close to the mass of our Sun. When a core exceeds the Jeans mass, it will start to collapse on a timescale comparable to the free-fall timescale

$$t_{\rm ff} \sim (G\rho)^{-1/2} \sim 10^5\ {\rm yr} \left(\frac{n}{10^4\ \rm cm^{-3}}\right)^{-1/2}, \tag{1.2}$$

with G the gravitational constant and $\rho = n\mu m_{\rm H}$ the gas density, written in terms of the mean molecular mass $\mu \simeq 2.34$ and the hydrogen mass $m_{\rm H}$. The collapse of a protostellar core is depicted in Fig. 1.2b. Describing the collapsing core as a sphere of uniform density in solid body rotation, and assuming typical ratio of rotational to gravitational energy of $\beta = 0.02$, we obtain a total angular momentum of $J_{\rm core} \sim 10^{54}$ g cm^2 s^{-1}, and a specific angular momentum of $l_{\rm core} \sim J_{\rm core}/M_\odot \sim 10^{20}$ cm^2 s^{-1}. Because of conversation of angular momentum, the infalling material will create a rotationally supported disk (Fig. 1.2c), the size of which can be estimated by looking at the specific angular momentum in a Keplerian disk

$$R_{\rm disk} = \frac{l_{\rm core}^2}{GM_\odot} \sim 100\ {\rm AU}. \tag{1.3}$$

These disks, dubbed circumstellar disks, protoplanetary disks, or protoplanetary nebula, are believed to be the sites of planet formation. The protoplanetary disk is clearly visible during phases d) and e) of Fig. 1.2, but might already be present in the earlier phases (e.g., Tobin et al. 2012; Murillo et al. 2013).

Assuming the disk is more or less axisymmetric, the general structure is described by a temperature $T(R,z)$ and density $\rho_{\rm g}(R,z)$, both functions of the radial distance to the star R, and the height above the midplane z. We focus first on the vertical structure. The gas is orbiting perpendicular to z, so there is no angular momentum keeping the gas from falling to the midplane as a result of the vertical component of the central star's gravity. Thus, for the disk to be supported vertically, a pressure gradient has to balance the gravitational force

$$c_s^2 \frac{{\rm d}\rho_{\rm g}}{{\rm d}z} = -\frac{GM_\star z}{(R^2+z^2)^{3/2}}\rho_{\rm g}, \tag{1.4}$$

with c_s the sound-speed, and $M_\star$ the mass of the central star. Assuming that the disk is vertically isothermal, i.e., $T(R,z) = T(R)$, and relatively flat, $z \ll R$, the solution can be obtained as

$$\rho(z) = \rho_{\rm g,0} \exp\left(-z^2/2h_{\rm g}^2\right), \tag{1.5}$$

with $\rho_{\rm g,0}$ the density in the midplane, $h_{\rm g} \equiv c_s/\Omega$ the vertical disk scale height, and $\Omega = (GM_\star/R^3)^{1/2}$ the Kepler frequency. The temperature structure can be approximated by a simple power law

$$T(R) = T_0 \left(\frac{R}{R_c}\right)^{-q}\ {\rm K}. \tag{1.6}$$

For optically thin disks, the radiation flux directly received by a part of the disk scales as $\mathcal{F} \propto 1/R^2$. Since $\mathcal{F} \propto T^4$, this results in an exponent $q = 1/2$ for the temperature power law. Similar values have been found observationally (e.g., Andrews & Williams 2005). Then, since $h_{\rm g} = c_s/\Omega$ and $c_s = (k_{\rm B}T/\mu m_{\rm H})^{1/2}$, we obtain $h_{\rm g}/R \propto R^{1/4}$, i.e., the 'opening angle' of the disk increases with radius; such disks are dubbed flaring disks. More complex models for the disk temperature can be constructed by taking into account radiative transfer, accretion, and dust opacities. Such models typically find that the mid-plane is considerably colder than the surface layer of the disk, as stellar photons with short wavelengths cannot penetrate this deep (e.g., Dullemond et al. 2007). The wide range of densities, temperatures, and UV-intensities leads to a wide range of complex chemistry, and variation in the gas-ice balance of volatiles (e.g., Dutrey et al. 2014; Pontoppidan et al. 2014). Of special importance for the dust evolution is the *snowline*, the location in the protoplanetary disk behind which volatiles freeze out onto solid dust grains. The resulting icy grains have very different sticking properties from bare silicate grains, which greatly influences their collisional evolution (Sect. 1.2). The location of the snow line depends on the stellar parameters and structure of the disk and the dust within it, but typically $R_{\rm snow} \sim 3$ AU (Min et al. 2011).

By integrating over the vertical direction, we obtain the gas surface density

$$\Sigma_{\rm g}(R) = \int_{\infty}^{\infty} \rho_{\rm g}(R,z)\,{\rm d}z = \sqrt{2\pi}\rho_{\rm g,0}h_{\rm g}. \tag{1.7}$$

It is customary to describe the gas surface density with a truncated powerlaw (Lynden-Bell & Pringle 1974; Hartmann et al. 1998a)

$$\Sigma_{\rm g}(R) = \Sigma_0 \left(\frac{R}{R_c}\right)^{-\gamma} \exp\left[-\left(\frac{R}{R_c}\right)^{2-\gamma}\right], \tag{1.8}$$

although observational constraints on the form of $\Sigma_{\rm g}(R)$ are poor, especially in the outer regions of the disk. The total disk mass equals

$$M_{\rm D} = 2\pi \int_0^{\infty} R\Sigma_{\rm g}\,{\rm d}R = \frac{2\pi}{(2-\gamma)}\Sigma_0 R_c^2 \tag{1.9}$$

provided $\gamma \neq 2$. The critical radius R_c is of the order of $R_{\rm disk}$ (Eq. 1.3), and there are several ways of constraining γ and/or $M_{\rm D}$. One is to look at how the solids are distributed in our own Solar System. By looking at the radial distribution of solids (mostly rocky planets and the cores of gas giants), and assuming a dust-to-gas ratio of 10^{-2}, one finds that $\Sigma(R) = R^{-3/2}$ is fairly accurate within 30 AU (the location of Neptune), with $\Sigma_{\rm g}(1\ {\rm AU}) = 1.7 \times 10^3$ g cm^{-3} (Weidenschilling 1977b; Hayashi 1981). This model is called the Minimum Mass Solar Nebula (MMSN), and yields a total disk mass of $\sim 10^{-2} M_\odot$. However, the MMSN model assumes a number of things that are not necessarily true; for example, it assumes the majority of solids originally present in the disk ended up in planets, and that these planets did not move (migrate) significantly after their formation. From observations, one finds $M_{\rm D}/M_\odot \simeq 10^{-3} - 0.2$ and $\gamma \simeq 0.9$ around Sun-like stars (Andrews et al. 2009).

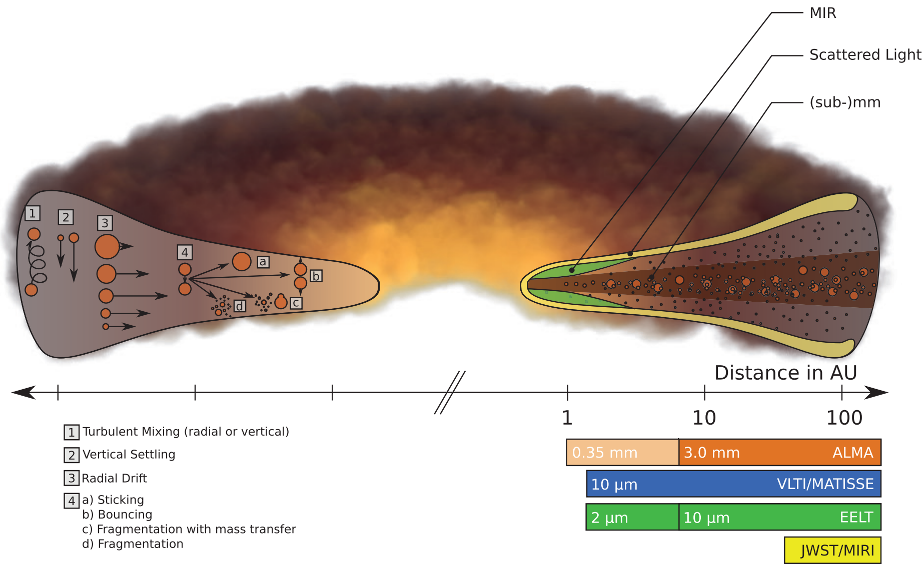

Figure 1.3: Schematic of a turbulent protoplanetary disk. On the left, various grain processes are illustrated: turbulent diffusion (1); settling (2); radial drift (3); and grain-grain collisions with different outcomes (4). On the right, the colored areas indicate which regions of the disk can be probed by which instrument/telescope. Figure from Testi et al. (2014).

If the gas disk itself is very massive, it can become gravitationally unstable, and collapse or fragment. The strength of the disk's self-gravity is described by the Toomre parameter

$$Q_{\rm T} \equiv \frac{c_s \Omega}{\pi G \Sigma}, \tag{1.10}$$

and disks with $Q_{\rm T} \geq 1$ are unstable. This condition can be rewritten as $M_{\rm D}/M_\star \gtrsim h_{\rm g}/R$. Typically $h_{\rm g}/R = 0.05 - 0.1$, and gravitational instability will only occur for the most massive disks.

1.1.2 Gas and dust evolution

The picture sketched in the previous paragraph might suggest the protoplanetary disk is a static, quiet environment. It is, however, anything but. The majority of protoplanetary disks are accreting matter onto the central star, with typical accretion rates anywhere between $\dot{M} \sim 10^{-10} - 10^{-7}\ M_\odot\ {\rm yr}^{-1}$ (e.g., Muzerolle et al. 2000). The accretion rate, and the timescale on which disks evolve in general, are related to the disk viscosity.

One source of viscosity are collisions between molecules; the resulting molecular viscosity equals $\nu_{\rm mol} \sim c_s \lambda_{\rm mfp}$, with $\lambda_{\rm mfp} \sim \mu m_{\rm H}/\rho_{\rm g}\sigma_{\rm mol}$ the gas molecule mean free path, and $\sigma_{\rm mol} \simeq 2 \times 10^{-15}\ {\rm cm}^2$ the molecular cross section. Plugging in the numbers for an MMSN disk, we obtain $\nu_{\rm mol} \sim 10^5\ {\rm cm}^2\ {\rm s}^{-1}$. This results in a viscous timescale of $t_{\rm vis} \sim R^2/\nu_{\rm mol} \sim 10^{13}$ yr, much longer than the timescales on which gas disks evolve (Sect. 1.1.4). Clearly, other sources of viscosity must be present. Without, for now, specifying the source, it is instructive to assume an effective, turbulent viscosity, which can be parametrized as (Shakura & Sunyaev 1973)

$$\nu_{\rm T} = \alpha c_s^2/\Omega, \tag{1.11}$$

with α a dimensionless parameter governing the strength of the turbulence. In this description, energy is put in at the largest scales (fluctuations with a size L, that evolve on timescales t_L), and trickles down to smaller scales. It makes sense to assume the turn-over time of the largest eddies is set by the orbital period, i.e., $t_L \sim \Omega^{-1}$. These largest eddies have velocities of $v_L = L/t_L$, and because $Lv_L \sim \nu_{\rm T}$, this leads to $v_L \simeq \alpha^{1/2} c_s$. At the bottom of the Kolmogorov cascade, the smallest eddies have a characteristic timescale $t_\eta = {\rm Re}^{-1/2} t_L$, where ${\rm Re} = \nu_{\rm T}/\nu_{\rm mol} \gg 1$ is the turbulence Reynolds number. For a steady-state accretion disk, one can show that $\dot{M} = 3\pi\Sigma_{\rm g}\nu_{\rm T}$. Thus, if α does not vary with radius, we find $\gamma = 1$ for the exponent of the surface density. Inserting numbers appropriate for an MMSN-like disk at 30 AU, one finds $\alpha \simeq 10^{-2}$ corresponds to an accretion rate of $10^{-7}\ M_\odot\ {\rm yr}^{-1}$, and a viscous timescale of about a million years.

The parametrization of Eq. 1.11 is very idealized and might not be accurate depending on the mechanism driving the turbulence. Furthermore, even if the turbulence can be parametrized locally, the strength of the turbulence (i.e., α) need not be constant in the radial and vertical direction. Various candidates have been proposed as sources for the turbulent viscosity, including self-gravity (Gammie 2001), magneto rotational instability (MRI) (Balbus & Hawley 1991), and baroclinic vortices (Klahr & Bodenheimer 2003; Klahr 2004). The current understanding of turbulence in relation to accretion in protoplanetary disks is reviewed in Turner et al. (2014).

Apart from accreting onto the central star, several other disk dispersal mechanisms are at work, including disk photo-evaporation and disk winds. A recent review on disk dispersal mechanisms is given by Alexander et al. (2014). Observations indicate a disk lifetime of ~3 Myr (Sect. 1.1.4), and put constraint on the efficiency of the disk removal mechanisms, but also on the timescales of giant planet formation, which must take place *before* the gas is dissipated (Pollack et al. 1996). Crudely, planet formation can be split into two stages: the formation of planetesimals out of microscopic dust grains (e.g., Testi et al. 2014; Johansen et al. 2014); and the subsequent formation of planets out of said planetesimals (e.g., Raymond et al. 2014). The word planetesimal usually refers to solid bodies with sizes of $\gtrsim$km, approximately the size above which self-gravity starts to play a role for their further evolution. Sect. 1.2 expands upon the journey from dust grain to planetesimal.

1.1.3 Evolved systems

After the disk gas has been removed, hopefully, a 'naked' planetary system remains (Fig. 1.2f). This phase lasts for the remainder of the lifetime of the central star, around ~10 Gyr for Sun-like stars.

Planetary systems

A large number of exoplanets has now been discovered and characterized with a variety of observational techniques (Fig. 1.1), and it is held that the average star in our galaxy is orbited by several planets (Lissauer et al. 2011). These findings challenge, and put to the test current models of planet formation, which have to explain the high occurrence rate and diversity of observed (exo)planets.

One example is the discovery of so-called *hot Jupiters*: planets with a mass comparable to Jupiter's on tight compact orbits, with orbital periods that can be as short as several days (the planets in the upper left part of Fig. 1.1). In an MMSN-like disk, these inner regions of a protoplanetary disk do not hold enough mass to form Jupiter-size planets. The existence of these hot Jupiters led to the realization that planets may migrate through a disk, or be scattered later.

Indeed, the current distribution of planets does not necessarily reflect their formation history exactly. First, newly-formed planets will interact with the disk, exchanging angular momentum. These interactions can cause the planets to move radially through the disk, crossing considerable distances. This *migration* can happen in both directions and at different rates, depending on the disk structure and mode of migration (Baruteau et al. 2014). Second, even after the gas has dissipated, the young planetary system might not be dynamically stable, and gravitational interactions between the planets (or even fly-by's of other stars) can result in dynamical instabilities, and major make-overs for the system's structure (e.g., Davies et al. 2014).

Debris disks

The final stage of planet formation is not necessarily efficient in all disks, or in all regions within a disk. In the Solar System for example, the asteroid belt, located between Mars and Jupiter, can be thought of as the remains of an unsuccessful attempt. It is believed that in this particular case, the many mean motion resonances with Jupiter prevented bodies from conglomerating further; but planet formation could be unsuccessful for many reasons, not all of them related to nearby planets. For example, the original protoplanetary disks might not have contained enough solids in the first place, or, the turbulence and temperature structure of the disk might have made it a hostile environment for the growing aggregates.

Many old systems have now been discovered that have so-called *debris disks*, rings of debris similar to our asteroid belt, but often more massive and at larger separations (see Matthews et al. 2014, for a complete review). In debris disks, the mass is usually dominated by large, (super)km-size bodies, invisible to our telescopes. In the absence of gas, these bodies suffer violent collisions resulting in a collisional cascade. At the bottom of this cascade, dust particles with sizes of $\sim\mu$m are created, which can be observed. In some of these systems, planets have been reported as well (Kalas et al. 2005, 2008; Marois et al. 2008; Lagrange et al. 2010).

1.1.4 Observational contraints

The star- and planet formation paradigm, as summarized by Fig. 1.2, can be tested directly by studying the solids in the Solar System, and indirectly by observing radiation from other systems.

Disk observations

Observations of young stellar objects provide valuable information about the properties of protoplanetary disks. Here, we only skim the surface of the field of disk observations, and refer the reader to Williams & Cieza (2011) and Testi et al. (2014) for extensive reviews.

Initially, because of their small angular size, protoplanetary disks could not be resolved, and their existence was inferred by studying the stellar spectral energy distribution (SED) (Beckwith et al. 1990). The spectrum of a Sun-like star peaks in the UV and the optical. When a disk surrounds the star however, significant flux is observed at longer wavelengths, ranging from the mid-IR, to mm-wavelenghts; the result of both reprocessing of stellar radiation, and of thermal emission of dust grains. The right-hand side of Fig. 1.3 shows approximately which regions of the disk emit mid-IR and mm emission. By looking at the fraction of stars in star clusters that show such excess radiation, a typical disk lifetime of ~3 Myr can be inferred (e.g., Haisch et al. 2001), though some studies suggest lifetimes beyond 10 Myr (Pfalzner et al. 2014).

Continuum observations at (sub)mm wavelengths probe the interior of the protoplanetary disk, where most of the dust mass is located. The flux at these wavelengths is dominated by thermal emission of the dust grains, and can be approximated as

$$\nu F_\nu \approx \nu \kappa_\nu B_\nu(T) \frac{M_\mathrm{d}}{R^2}, \tag{1.12}$$

with $B_\nu(T)$ the temperature-dependent Planck function, ν the frequency, κ_ν the dust opacity (per unit mass), and M_d the total dust mass. By measuring the flux at multiple wavelengths, it is possible to constrain the slope of the opacity function $\kappa_\nu \propto \nu^\beta$, where β is called the spectral index. At (sub)mm wavelengths, the spectral index β depends on the dust properties and its size-distribution, and can be used to constrain grain growth (Natta & Testi 2004; Natta et al. 2007; Wilner et al. 2005; Ricci et al. 2010). Furthermore, when the disk can be resolved angularly, observed variations in β can provide clues about how grain growth varies with location in the disk (e.g., Pérez et al. 2012). However, interpretation of mm-observations is a precarious business, as the spectral index varies greatly with not just particle size and distribution, but also grain chemical composition and porosity (Cuzzi et al. 2014; Kataoka et al. 2014), and grain temperature (Demyk et al. 2012).

Now, facilities such as the Atacama Large Millimeter Array (ALMA), the Very Large Telescope Interferometer (VLTI), and soon the James Webb Space Telescope (JWST), are able to resolve protoplanetary disks down to scales approaching a few AU at micrometer-millimeter wavelengts (see also Fig. 1.3). Such high-resolution observations reveal the distribution of matter in disks, and variations in the disk's structure at smaller and smaller scales. So far, these observations have revealed coherent spatial structures such as gaps, spiral arms, and azimuthal asymmetries in the disk and dust structure (e.g., van der Marel et al. 2013; Casassus et al. 2013; Pérez et al. 2014), possibly signs of planet formation in action. Furthermore, tentative direct observations of young (forming) planets inside protoplanetary disks confirm these disks are the principle sites of planet formation (Kraus & Ireland 2012; Quanz et al. 2013).

Solar System

As an evolved system, our own Solar System holds clues to its formation history. Some obvious, some less so. First, there are the planets; we already saw how the distribution of planets led to the concept of the Minimum Mass Solar Nebula. Focussing on the properties of the planets, we notice a dichotomy: small rocky planets in the inner Solar System, and massive gas giants in the outer parts. The division occurs somewhere between Mars and Jupiter, and it is tempting to attribute this devision to the location of the snow line.

Moving to much smaller objects, a tremendous amount of information can be obtained from studying meteorites (e.g., Russell et al. 2006; Connelly et al. 2012), small chunks of asteroids that fall onto Earth. The largest class of meteorites are the chondritic meteorites, which constitute the oldest known undifferentiated bodies in the Solar System. These chondrites consist of three components: chondrules, calcium-aluminum-rich inclusions (CAIs), and matrix material. Chondrules are spherical silicate crystals with sizes between $\sim 50\,\mu$m and several mm, and are the dominant component in meteorites. CAIs are slightly larger, with sizes $\lesssim$cm, but less common. The matrix material is composed of (sub)micron-size silicate grains, and fills the spaces between the chondrules (and CAIs). Of these components, the CAIs are the oldest, and are believed to be the first condensates in the Solar System. Radioactive dating places the formation of the CAIs at 4.567 Gyr ago, while differences between CAIs indicate they formed during an interval of ~0.25 Myr. Dating indicates chondrules formed over a period of ~2 Myr, starting $1-2$ Myr after the formation of the CAIs. It is now held that chondrules also formed earlier, perhaps together with CAIs, but that these early chondrules were incorporated into parent bodies that underwent differentiation (the magmatic iron meteorites). The spread in formation ages between CAIs and chondrules suggest coagulation and planetesimal formation occurred over several Myrs, a timespan comparable to the typical age of a protoplanetary disk. Another interesting finding is that while chondrule sizes vary between meteorites, their size distribution within a single parent body is relatively narrow. This seems to indicate that a size-sorting mechanism was acting in the early protoplanetary disk; and that the parent bodies formed only after some sorting was done. Much more can be learned from the primitive materials in our Solar System, and the interested reader is referred to the recent review of Gail et al. (2014).

1.2 From dust to planetesimal

For the formation of planets, the accumulation of solids is key. The molecular clouds of the previous section form out of the tenuous interstellar medium (ISM). Thus, like the ISM, about 1% of their mass is in solid dust particles; typically particles with sizes $\lesssim$0.3 μm (Mathis et al. 1977). Because of the high densities in the disk midplane, these grains can collide and grow to larger sizes. Here, we discuss the main processes that govern the growth of these particles towards, eventually, planetesimal sizes.

1.2.1 Dynamics of dust grains

The dynamics of small dust particles, suspended in a young protoplanetary disk, are governed mainly by their interaction with the turbulent gas. An important concept is the particle stopping time t_s, which describes how much time is needed for a dust particle to loose its momentum due to friction with the surrounding gas. The stopping time is often multiplied by the orbital frequency to form the *Stokes number*, Ωt_s, a dimensionless quantity.

Imagine a dust particle with a size a, and mass m. Depending on the size of the particle with respect to the gas mean free path, the stopping time is set either by Epstein or Stokes drag

$$t_s = \begin{cases} t_s^{(\mathrm{Ep})} = \dfrac{3m}{4\rho_\mathrm{g} v_\mathrm{th} A} & \text{for } a < \dfrac{9}{4}\lambda_\mathrm{mfp}, \\[2ex] t_s^{(\mathrm{St})} = \dfrac{4a}{9\lambda_\mathrm{mfp}} t_s^{(\mathrm{Ep})} & \text{for } a > \dfrac{9}{4}\lambda_\mathrm{mfp}, \end{cases} \tag{1.13}$$

where $v_\mathrm{th} = \sqrt{8/\pi} c_s$ is the mean thermal velocity of the gas molecules, and $A \simeq \pi a^2$ is the particle's cross section. In the midplane at 5 AU, $\lambda_\mathrm{mfp} \sim 1$ m, and small dust grains are always in the Epstein regime.

While the gas is supported by a vertical pressure gradient, there is nothing stopping the dust grains from settling to the midplane of the protoplanetary disk. By comparing the vertical component of the stellar gravity to the gas drag experienced by a particle, one obtains the terminal settling velocity $v_z = \Omega^2 z t_s$ with z the height above (or below) the midplane. The timescale for settling then equals $t_\mathrm{sett} = (\Omega^2 t_s)^{-1}$. At 1 AU, a millimeter-size dust particle has $t_\mathrm{sett} \sim 10^2$ yr, very short compared to the disk lifetime. However, the presence of turbulence will lead to particles diffusing (back) to the upper layers of the disk. For relatively well-coupled particles, the diffusion timescale equals $t_\mathrm{diff} \sim (\alpha\Omega)^{-1}$. Particles for which the diffusion timescale is shorter/comparable to the settling timescale, i.e., with $t_s \leq \alpha/\Omega$, will not settle efficiently, and inhabit the same volume as the gas. Particles that are more decoupled will settle into a disk with a scale height (Youdin & Lithwick 2007)

$$\frac{h_\mathrm{d}}{h_\mathrm{g}} = \left(1 + \frac{\Omega t_s}{\alpha} \frac{1 + 2\Omega t_s}{1 + \Omega t_s}\right)^{-1/2}, \tag{1.14}$$

where $h_\mathrm{d}/h_\mathrm{g} \leq 1$.

Apart from settling to the midplane, largish grains will also drift radially towards the central star. The reason for this is that large grains, orbiting on Keplerian orbits, loose angular momentum to the gas, which is orbiting at a slightly sub-Keplerian velocity because of the radial pressure gradient. As a result, grains drift inward with a velocity (Weidenschilling 1977a)

$$v_{\rm drift} = -\frac{2\Omega t_s}{1+(\Omega t_s)^2}\eta v_{\rm K}, \tag{1.15}$$

where an important quantity is the dimensionless pressure gradient η, defined as (Nakagawa et al. 1986)

$$\eta \equiv -\frac{1}{2}\left(\frac{c_s}{v_{\rm K}}\right)^2 \frac{\partial \ln(\rho_{\rm g} c_s^2)}{\partial \ln R}. \tag{1.16}$$

with $v_{\rm K} = R\Omega$ the Keplerian orbital velocity. The timescales on which decoupled particles drift in can be quite short, and radial drift poses a serious problem for further growth (Sect. 1.2.3).

Finally, an important concept for coagulation is the dust particle relative velocity, i.e., the velocity at which two grains with masses m_1 and m_2 collide. For (sub)micrometer grains, the relative velocity is dominated by Brownian motion, and given by

$$\Delta v_{\rm BM} = \sqrt{\frac{8k_{\rm B}T(m_1+m_2)}{\pi m_1 m_2}}, \tag{1.17}$$

with $k_{\rm B}$ the Boltzmann constant. For these small grains, the relative velocity $\Delta v_{\rm BM} \sim$ mm s^{-1}, but quickly decreases with increasing mass. For larger grains, an important source for relative velocities is the turbulence. Relative velocities resulting from interaction with the turbulent eddies are challenging to calculate. Based on the work of Voelk et al. (1980), closed-form expression were derived by Ormel & Cuzzi (2007), as a function of the stopping times of both particles. An important notion is that the largest turbulent-induced relative velocities are achieved when $\Omega t_s \sim 1$, in which case $\Delta v_{\rm turb} \sim \alpha^{1/2} c_s$. In addition, when two aggregates have very dissimilar stopping times, their different drift and settling rates can be an important source of relative velocities. Differential drift velocities also peak at a Stokes number of unity, at $\Delta v_{\rm drift} \sim \eta v_{\rm K}$.

1.2.2 Coagulation

Assuming all dust particles have similar properties (i.e., mass, size, stopping time), and stick together upon colliding, the growth timescale is given by

$$t_{\rm grow} \sim \frac{1}{n_{\rm d}\sigma_{\rm coll}\Delta v}, \tag{1.18}$$

with $n_{\rm d}$ the dust particle number density, Δv the relative velocity between the dust particles, and $\sigma_{\rm coll}$ the collisional cross section. Thus, simply speaking, growth is fastest when densities are high, collisional cross sections are large, and relative velocities are high.

1.2.3 Growth barriers

There are several obstacles (or barriers) that have to be overcome by growing dust grains in order to become planetesimals. In general, there are two distinct types of growth barriers: one pertaining to the collisional outcomes; the other involving rapid removal of the dust particles from the disk.

Collisional barriers

When particles collide at high velocities, sticking will not be the most likely outcome, and particles are more likely to bounce of each other, or even destroy and fragment. Over the last two decades, a wealth of collision experiments has been collected in order to identify exactly at which velocities growth is possible (see Blum & Wurm 2008, for an in-depth review). For silicates, Güttler et al. (2010) have combined this 'zoo' of experiments into the so-called *Braunschweig collision model*. In this model, colliding grains are divided into 'porous' and 'compact' grains, and collisions are either between 'similar-size' or 'different-size' particles; resulting in 8 possible collision types. Based on the large collection of experiments, Güttler et al. (2010) then provided maps for each collision type, showing, as a function of particle mass and velocity, where sticking, bouncing, and fragmentation are expected to occur. For ices, experimental studies become increasingly challenging, mainly because of the low temperatures that have to be maintained during the preparation and execution of the collision experiments. Nonetheless, experimental results are becoming available (Gundlach et al. 2011; Aumatell & Wurm 2014), indicating microscopic icy particles can achieve sticking at very high velocities (Gundlach & Blum 2015).

The velocity above which sticking is unlikely depends on many factors, some of which will be discussed in more detail in Sect. 1.3; but as a rough estimate, compact mm-size aggregates of refractory particles tend to bounce at velocities $\gtrsim$1 cm s^{-1}, and fragment above $v_{\rm frag} \sim 1$ m s^{-1}. In the inner regions of protoplanetary disks typical collision velocities are well above the fragmentation velocity for silicate particles. In general, full models of dust coagulation find that, when dust grains are assumed to be compact at all times, the bouncing and fragmentation prevent dust particles from growing much larger than ~cm (e.g., Brauer et al. 2008a; Birnstiel et al. 2010; Testi et al. 2014). However, experiments suggest that grains might still gain mass in destructive collisions with smaller particles (Wurm et al. 2005; Kothe et al. 2010). Such mass-transfer might then allow these larger bodies to grow further (Windmark et al. 2012a).

In the cold outer regions, where sticky ices are present, the relative velocities are lower (the turbulent velocity $\Delta v_{\rm turb} \propto c_s^{1/2}$ decreases with disk radius). In addition, porous icy aggregates are stickier, and can dissipate collisional energy more easily. A bouncing regime is then not expected for these aggregates, and the transition between sticking and fragmentation occurs at several tens of m s^{-1}. These icy aggregates are expected to survive collisions with similar-size particles, offering a pathway for further growth (Okuzumi et al. 2012).

The drift barrier

In the previous section it was shown that marginally decoupled grains will drift inward with a velocity $v_{\rm drift}$ (Eq. 1.15). The drift timescale $t_{\rm drift} = R/v_{\rm drift}$ is shortest for grains with $\Omega t_s = 1$, for which $t_{\rm drift} \sim (\eta\Omega)^{-1}$. Typically $\eta \sim 10^{-2}$, which means the drift timescale can be very short indeed, $\sim$100 orbital periods. In other words, grains with $\Omega t_s \sim 1$, situated around 1 AU from a Sun-like star, will drift inward on a 100 yr timescale (Weidenschilling 1977a). This rapid removal of grains is often referred to as the radial drift barrier.

Several ways have been suggested to circumvent the drift barrier. First, the existence of pressure bumps in the gas disk can locally decrease (or even invert) the pressure gradient, trapping particles in the pressure maxima (e.g., Kretke & Lin 2007; Pinilla et al. 2012a,b) (see also Sect. 1.2.4). Second, if the growth timescale is (much) shorter than the timescale for drift, i.e., $t_{\rm grow} < t_{\rm drift}$, particles can outgrow the radial drift problem (Okuzumi et al. 2012). For this to work, aggregates with $\Omega t_s \sim 1$ must be able to grow through collisions, despite the the fact that relative velocities peak at these Stokes numbers.

1.2.4 Particle concentration mechanisms

The growth timescale of Eq. 1.18 depends on the dust particle number density. If the dust and gas are well-mixed, the mass density of dust particles is roughly $\rho_{\rm d} \sim \Sigma_{\rm d}/h_{\rm d}$, and increases when grains settle to the midplane. There exist however several particle concentration mechanisms that can locally and/or temporarily increase $n_{\rm d}$ much further, potentially leading to rapid growth. First, tightly-coupled particles ($t_s \sim t_\eta$) can accumulate in the high-pressure regions between the smallest turbulent eddies (Cuzzi et al. 2001, 2008), though the total mass present in these particle concentrations might be small (Pan et al. 2011). Second, pressure bumps or vortices, giving rise to variations of the order $h_{\rm g}$, can effectively concentrate particles with $0.1 < \Omega t_s < 10$ (e.g., Kretke & Lin 2007), though it is not clear how common such bumps and/or vortices are. Finally, populations of bodies with $10^{-2} < \Omega t_s < 1$ can result in streaming instability, and collapse to form planetesimals in a timescale compared to the orbital period (Youdin & Goodman 2005; Johansen et al. 2007; Bai & Stone 2010a,b). For this to be possible, a dense midplane layer of solids is required, where the dust-to-gas ratio is approximately unity. These concentration mechanisms are described in more detail in Johansen et al. (2014).

In summary, the turbulent gas disk is a complex environment, and the interplay between dust and gas can give rise not only to growth barriers, but also to particle concentration mechanisms that are beneficial for growth. The efficiency of these mechanisms however, depends sensitively on the aerodynamical properties of the present dust grains.

1.3 Dust microphysics

The microphysical structure of dust aggregates plays a major role in their (collisional) evolution. First, the microstructure profoundly influences the aggregate's mechanical properties, and therefor the collisional outcomes. For example, highly porous aggregates can dissipate collision energy more easily, and are less likely to bounce. Second, the shape and size of an aggregate influence its coupling to the gas, changing the particle's stopping time, thus influencing the settling/drift behavior, collision velocities, and efficiency of particle concentration mechanisms. Finally, porosity influences grain opacities (i.e., κ_ν in Eq. 1.12), changing the appearance of dust in disks. It is clear then that an intimate understanding of the porosity evolution of dust aggregates is needed to understand the details of dust coagulation (the first stages of planetesimal formation), and to accurately interpret observations of dust in protoplanetary disks.

Two quantities are often used to describe the structure of porous aggregates; the first is the filling factor ϕ, which represents the fraction of the aggregate's volume that is taken up by solids. A solid sphere has $\phi = 1$, and the maximum filling factor of an aggregate made up of mono disperse spheres is $\phi \simeq 0.74$. Depending on the specifics of the growth process, the filling factor of aggregates in astrophysical environments may be $\ll 1$. The second parameter is the fractal dimension δ_f, which relates the mass and the size of the aggregate through

$$m = k_f \left(\frac{a}{r}\right)^{\delta_f}, \tag{1.19}$$

with r the monomer radius. The fractal dimension can range from anywhere between 1 (for linear chains) to 3 (for homogeneous particles). It should be noted that $\delta_f \simeq 3$ does not necessarily imply a compact aggregate, since k_f can still be very small.

1.3.1 Early growth

Initially, the microscopic grains present in the protoplanetary disk collide very gently, at velocities set by Brownian motion. When small grains meet at these velocities, they readily stick together as the result of attractive surface forces. In this low-velocity hit-and-stick regime, two modes of growth can be identified: one where aggregates grow by colliding with same-size partners (CCA for cluster-cluster aggregation); and one where aggregates grow by sweeping up small grains (PCA for particle-cluster aggregation). During CCA growth, very open, porous aggregates are formed, that evolve with $\delta_f \approx 2$, as found by experimental studies (Blum et al. 2000; Krause & Blum 2004) and theoretical work (Ossenkopf 1993; Kempf et al. 1999). This fractal growth is generally held to be an accurate description of the start of the coagulation process in protoplanetary disks.

As the fluffy aggregates gain mass, the turbulence and differential settling begin to dominate their collision velocities, which tend to increase. Then, as grains collide with more momentum, collisions will be energetic enough to start to restructure the aggregates, possibly compacting them. A schematic of hit-and-stick growth and compaction is shown in Fig. 1.4. As illustrated in panel (b), hit-and-stick growth leads to the addition of voids to the aggregate's structure, leading to a decrease in ϕ, while the fractal dimension stays constant at $\delta_f \approx 2$. In the case of aggregate compaction (Fig. 1.4c), the changes in the internal structure are more complex, and the most popular methods to study this process have been so-called molecular dynamics simulations.

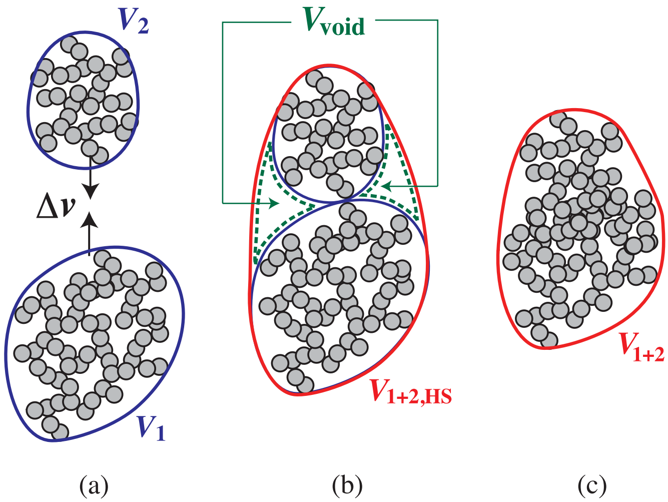

Figure 1.4: Sticking of porous aggregates. (a) Two aggregates, with volumes V_1 and V_2, collide at a velocity Δv. (b) At low velocities, the collision results in sticking without restructuring. Voids are added, and the total volume of the resulting aggregate is $V_{1+2,\text{HS}} > V_1 + V_2$. (c) At higher collision velocities, significant restructuring takes place, and $V_{1+2} < V_{1+2,\text{HS}}$. Figure from Okuzumi et al. (2012).

1.3.2 Molecular dynamics simulations

One way to study the effects of restructuring, is to perform dynamic simulations that resolve the (internal) forces between the aggregate's constituents during a collision. Dominik & Tielens (1997) were the first to tackle coagulation using such an approach. In their seminal paper, Dominik & Tielens simulated collisions between aggregates composed of $\lesssim$100 micron-size monomers at a range of velocities, and defined various collision regimes, based on the characteristic energies of the monomer-monomer contact. The various regimes are shown in Table 1.1. The two characteristic energies E_{break} and E_{roll} correspond, respectively, to the breaking of a single adhesive bond, and to the rolling of one monomer over another monomer by 90°. The value of these critical energies depends on monomer size and material, and will be discussed further in Sect. 1.3.3. Blum & Wurm (2000) found their experimental results on sticking, restructuring, and fragmentation of silicate aggregates to be in qualitative agreement with the picture drawn in Table 1.1, adding that theory and experiments were in agreement when the critical energies were adjusted by some factors of 10.

The work of Dominik & Tielens sparked many follow-up studies, involving an ever-increasing number of monomers N. Studies have been performed looking at the mechanical properties of aggregates (e.g., Paszun & Dominik 2008; Seizinger et al. 2012; Kataoka et al. 2013b); specifically looking at collisions between rotating partners (Paszun & Dominik 2006); investigating the bouncing behavior of aggregates (Wada et al. 2011;

Collision energy	Outcome of collision
$E_{\mathrm{K}} < 5E_{\mathrm{roll}}$	Sticking without restructuring
$E_{\mathrm{K}} > 5E_{\mathrm{roll}}$	Onset of compaction
$E_{\mathrm{K}} \sim n_c E_{\mathrm{roll}}$	Maximum compression
$E_{\mathrm{K}} > n_c E_{\mathrm{break}}$	Loss of some monomers
$E_{\mathrm{K}} > 10 n_c E_{\mathrm{break}}$	Catastrophic disruption

Table 1.1: Collision outcomes for roughy equal-size aggregates in terms of the characteristic energies E_{break} and E_{roll}, and the total number of contacts n_c. Based on Dominik & Tielens (1997, Table 3).

Seizinger & Kley 2013); focussing on the porosity evolution of aggregates in head-on collisions (Wada et al. 2007, 2009; Suyama et al. 2008, 2012) and offset collisions (Paszun & Dominik 2009); and examining the transition from growth to mass-loss with increasing collision velocity (Wada et al. 2013). Fig. 1.5 shows how numerical aggregates have evolved from 2D structures[1] with $N \sim 10^2$, to 3D aggregates with $N \sim 10^6$ (e.g., Wada et al. 2013). With monomer radii typically between $0.1 - 1\ \mu$m, the largest of these aggregates have sizes $\lesssim 100\ \mu$m. Even though larger aggregates are challenging to simulate, universal scaling laws can be obtained from the large collections of simulations. Recently, Okuzumi et al. (2012) and Suyama et al. (2012) developed expressions for the total volume of a newly-formed porous aggregate, based on the collision velocity, and the properties of the colliders. They found that aggregates that grow through subsequent compressive collisions with ~same-size partners can maintain a highly porous structure, with a nearly constant porosity that can be as low as $\phi \sim 10^{-5}$ for aggregates consisting of submicron icy monomers. Another interesting outcome of these simulations has been that bouncing is only possible for aggregates whose coordination number (the average number of contacts per monomer) is higher than ~6. In terms of porosity, this corresponds to $\phi \gtrsim 0.3$ (Wada et al. 2011; Seizinger & Kley 2013).

Full coagulation models that include particle porosity as a second property (in addition to particle mass) confirm that porosity matters a lot (Ormel et al. 2007; Okuzumi et al. 2009; Zsom et al. 2011). If particles can keep on growing highly-porously, which ice aggregates might, rapid growth through the drift barrier could even be possible (Okuzumi et al. 2012).

1.3.3 Radial and lateral forces

The main physical ingredient of the simulations of the previous section are the laws that describe the various inter-monomer forces. Long-range forces such as gravity or electrostatic forces are usually not included, and monomers can only exchange forces when they are touching. When two grains are in contact (i.e., touching), 4 principle modes of

[1]It should be noted that, despite the subsequent addition of a third spatial dimension and the enormous increase in the simulated number of monomers, the aggregates of Dominik & Tielens (1997) remain the only ones in which the monomers had a distribution of radii, rather than being mono disperse.

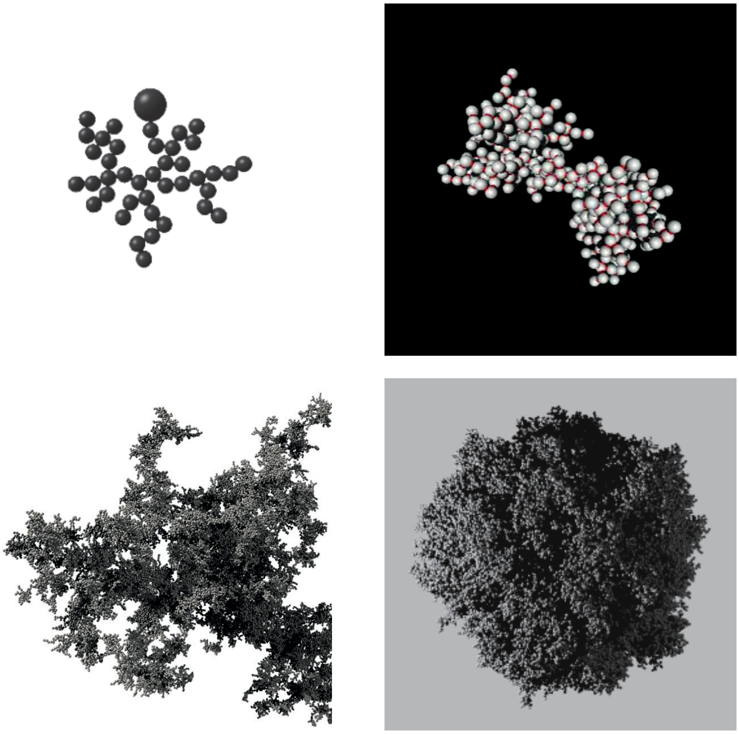

Figure 1.5: Improvements in numerical modeling of dust aggregates. *Top left:* Two-diminsional aggregate consisting of 40 monomers (Dominik & Tielens 1997). *Top right:* Aggregate consisting of 200 monomers (Paszun & Dominik 2009). *Bottom left:* Fractal aggregate consisting of 6×10^4 monomers (Seizinger et al. 2013). *Bottom right:* Relatively compact aggregate consisting of 1.28×10^5 monomers (Wada et al. 2013). Images not to scale.

motion can occur: radial motion, rolling motion, sliding motion, and twisting (Fig. 1.6). Prescriptions for the individual forces were obtained by Chokshi et al. (1993); Dominik & Tielens (1995, 1996), and summarized in Dominik & Tielens (1997). These descriptions were based on the Johnson-Kendall-Roberts (JKR) model of an adhesive and perfectly elastic contact (Johnson et al. 1971; Johnson 1987).

The JKR contact model is an extension of the non-adhesive theory of Hertz (1882). Hertz imagined two perfectly elastic spheres of radii r_1 and r_2. When the two spheres are pressed together, a circular contact area with a radius a is created, and the spheres are compressed slightly, so that their centers of mass ($\vec{x}_1$ and $\vec{x}_2$) are separated by less then $r_1 + r_2$. Then, the mutual approach can be defined as $\delta = r_1 + r_2 - |\vec{x}_1 - \vec{x}_2| > 0$. By looking at the elastic energy stored in such a configuration, Hertz derived the repulsive

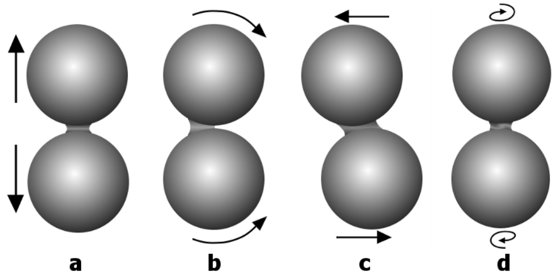

Figure 1.6: Main modes of motion in an adhesive contact between (sub)micrometer-size adhesive monomers: (a) radial (i.e., normal) motion, (b) rolling, (c) sliding, and (d) twisting. Figure from Seizinger et al. (2013), after Dominik & Tielens (1997).

radial force between two spheres to equal

$$F_{\rm H} = \frac{4E^* a^3}{3r}, \tag{1.20}$$

while the size of the contact being related to the approach through $a^2 = r\delta$, and typically $\delta \ll a \ll r$. Here, the elastic properties of the spheres are described in a single combined elastic modulus E^*, and $r^{-1} = r_1^{-1} + r_2^{-1}$ is the reduced radius. For a finite contact radius, $F_{\rm H} > 0$, and thus, the spheres will move apart in the absence of additional forces.

For microscopic bodies however, attractive surface forces can play an important role. By realizing that the presence of a mutual contact area results in a reduction of the total surface energy $\Delta U_S = \pi a^2 \gamma$, with γ the mutual surface energy, Johnson et al. (1971) obtained

$$\delta = \frac{a^2}{r} - \sqrt{2\pi\gamma a/E^*}, \tag{1.21}$$

and

$$F_{\rm JKR} = \frac{4E^* a^3}{3r} - \sqrt{8\pi\gamma E^* a^3}. \tag{1.22}$$

These relations are qualitatively different from the ones obtained by Hertz. First, the force can change signs, i.e., become attractive, for certain combinations of δ and a. As a result, there now exists an equilibrium solution where $F_{\rm JKR} = 0$ but the contact area is finite, given by

$$a_{\rm JKR} = \left(\frac{9\pi\gamma r^2}{2E^*}\right)^{1/3}. \tag{1.23}$$

Second, contact can persist at negative values of δ. Physically, this means that when spheres are pulled apart, a 'neck' of material will be formed that keeps the spheres in contact even for $\vec{x}_1 - \vec{x}_2 > r_1 + r_2$. When this neck becomes too long, the situation becomes unstable, contact is lost, and the spheres return to their spherical shape. The force needed to achieve pull-off equals $F_c = (3/2)\pi\gamma r$, independent of elastic properties.

These two effects have the consequence that a finite amount of energy has to be provided to break an existing bond. This energy is roughly

$$E_{\text{break}} \sim \left(\frac{\gamma^5 r^4}{E^{*3}}\right)^{1/3}. \tag{1.24}$$

Thus, contacts between sticky (high γ), soft (low E^*) materials cost more energy to break. When two monomers collide head-on, they will stick and remain together if the initial kinetic energy $E_{\text{K}} \leq E_{\text{break}}$. Equating these two energies results in a sticking velocity $v_{\text{stick}} \propto r^{-5/6}$; in other words, smaller spheres stick at higher velocities. Comparing ices and silicates, these considerations predict particles made of ice stick at velocities $\sim$10 times higher than silicate particles of a similar size.

When a lateral force is applied to center of mass of the sphere, a torque about the contact area is created. Starting from the JKR adhesive contact, Dominik & Tielens (1995) derived the critical rolling energy

$$E_{\text{roll}} = 6\pi\gamma r\xi, \tag{1.25}$$

as the energy needed to roll two spheres over each other over 90°. Here, ξ is the *rolling displacement*, related to the asymmetry of the contact area during the rolling motion. Dominik & Tielens connected the displacement to the intermolecular length scale, i.e., $\xi \sim 0.1$ nm.

Recent developments in molecular dynamics simulations have focussed on the ability to include an increasing number of monomers, and the contact description has not evolved much since its introduction in Dominik & Tielens (1997), despite a number of discrepancies with experimental results. First, the sticking velocity of individual monomers has been measured by Poppe et al. (2000) to be around $v_{\text{stick}} \simeq 1$ m s^{-1} for micron-size silicate grains, while the sticking velocity estimated from JKR theory is roughly 10 times lower. Second, the experimentally obtained rolling forces of Heim et al. (1999) indicate a value of $\xi \gg 0.1$ nm. Several reasons have been suggested for these discrepancies, including elastic waves, surface roughness, and deviations from elasticity, with many of the subsequent molecular dynamics simulations employing additional numerical factors to remove the disagreement with theoretical predictions.

1.4 This thesis

In this introduction we started from scales of $\sim$100 AU, corresponding to the typical size of a protoplanetary disk, and slowly worked our way down to through planets, planetesimals, dust grains, and eventually monomers, to eventually argue that the physical properties of the adhesive contact (corresponding to a scale $\lesssim\mu$m) are important for the early phases of planet formation. In the remainder of this thesis, we will walk the opposite route; starting from studying a single monomer-monomer contact (Chapters 2 and 3), we simulate dust coagulation in a local part of a nebula (Chapter 4), and finally study the global evolution of dust in a full protoplanetary disk (Chapter 5), before making a short excursion into the much older debris disk systems (Chapter 6).

The JKR model of an adhesive contact assumes the spheres are perfectly elastic, and that the contact area is in equilibrium. The size of the contact area is then found by minimizing the total surface- and elastic energy. Collisions however, are very dynamic processes, with typical durations of the order of 10^{-8} s for μm-size spheres. Furthermore, deviations from perfect elasticity are expected for realistic materials. In Chapter 2, we set out to extend the contact model to include dissipation of energy in the bulk of the colliding materials, and at the periphery of the adhesive contact. The new viscoelastic contact model is tested by comparing the predicted sticking velocity, and coefficients of restitution to a large set of published experiments on head-on collisions of small spheres.

In Chapter 3, we build on the viscoelastic model, and use it to re-evaluate the rolling force between adhesive monomers (i.e., Fig. 1.6b). The main goal is to achieve a better understanding of the rolling displacement parameter ξ (Eq. 1.25).

After these excursions into the world of contact mechanics, Chapter 4 constitutes the return to astronomy. In this chapter, the collisional evolution of a population of dust particles (initially all submicron grains) in a single column outside the snow line of a protoplanetary disk is studied. Coagulation is simulated using a special Monte Carlo technique (based on Ormel & Spaans 2008) that allows us to resolve the entire mass distribution, even parts that hardly contribute to the total dust mass budget. As the aggregates grow through collisions, the evolution of their filling factor is calculated self-consistently, as it is influenced by collisions, and non-collisional forces such as gas-drag or self-gravity. The main goal of this chapter is to determine whether erosion, caused by high-velocity impacts of small grains, can halt the rapid growth of porous aggregates through the radial drift barrier. In addition to the full Monte Carlo simulations, a semi-analytical model is introduced that is capable of capturing the evolution of the mass-dominating particles.

In Chapter 5, this semi-analytical model is developed further, and a new method is introduced to simulate the evolution of the dust surface density on a global scale, as it is changed by the combination of (porous) coagulation and radial drift. The method is used to study the formation of the first generation of planetesimals, the generation that is capable of forming out of a smooth gaseous nebula. Focussing on Sun-like stars, we study where in the disk porous coagulation can result in the formation of planetesimals, either through direct coagulation, or through streaming instability (Sect. 1.2.4) following coagulation/erosion equilibrium.

Chapter 6 takes a different perspective on the particles in debris disks, and addresses the lower end of the particle size distribution in these evolved systems. In debris disks (Sect. 1.1.3), the mass is typically dominated by km-size objects while the surface area of the solids resides in small dust particles, the results of a collisional cascade. In this chapter, we investigate which processes determine the observed cut-off of the particle size distribution around a few micrometer.

Finally, in Chapter 7, the main results of this thesis are summarized and promising avenues for future work are discussed.